

Limitations to the “basic” HOD model and beyond

Boryana Hadzhiyska,^{1*} Sownak Bose,¹ Daniel Eisenstein,¹
Lars Hernquist¹ and David N. Spergel^{2,3}

¹*Harvard-Smithsonian Center for Astrophysics, 60 Garden St., Cambridge, MA 02138, USA*

²*Department of Astrophysical Sciences, Princeton University, Princeton, NJ 08540 USA*

³*Center for Computational Astrophysics, Flatiron Institute, 162 Fifth Avenue, New York, NY 10010, USA*

Accepted XXX. Received YYY; in original form ZZZ

ABSTRACT

We make use of the IllustrisTNG cosmological, hydrodynamical simulations to test fundamental assumptions of the mass-based Halo Occupation Distribution (HOD) approach to modelling the galaxy-halo connection. By comparing the clustering of galaxies measured in the 300 Mpc TNG box (TNG300) with that predicted by the standard (“basic”) HOD model, we find that, on average, the “basic” HOD model underpredicts the real-space correlation function in the TNG300 box by $\sim 15\%$ on scales of $1 \text{ Mpc}/h < r < 20 \text{ Mpc}/h$, which is well beyond the target precision demanded of next-generation galaxy redshift surveys. We perform several tests to establish the robustness of our findings to systematic effects, including the effect of finite box size and the choice of halo finder. In our exploration of “secondary” parameters with which to augment the “basic” HOD, we find that the local environment of the halo, the velocity dispersion anisotropy, β , and the product of the half-mass radius and the velocity dispersion, $\sigma^2 R_{\text{halfmass}}$, are the three most effective measures of assembly bias that help reconcile the “basic” HOD-predicted clustering with that in TNG300. In addition, we test other halo properties such as halo spin, formation epoch and halo concentration. We also find that at fixed halo mass, galaxies in one type of environment cluster differently from galaxies in another. We demonstrate that a more complete model of the galaxy-halo connection can be constructed if we combine both mass and local environment information about the halo.

Key words: cosmology: large-scale structure of Universe – galaxies: haloes – methods: numerical – cosmology: theory

1 INTRODUCTION

The standard Λ CDM model predicts that galaxies form and evolve in virialized structures made up of dark matter (DM) called halos. The investigation of the relationship between galaxies and their parent (host) halos is of vital importance for constraining fundamental cosmological parameters and for studying galaxy formation in detail. This is the case because the dark matter component is not directly observable, so one way to extract information about it is by observing the galaxies and their distributions. One of the standard and computationally inexpensive approaches that is used to study the galaxy distribution is the halo occupation distribution (HOD) model (Peacock & Smith 2000; Seljak 2000; Scoccimarro et al. 2001; Berlind & Weinberg 2002), which determines (probabilistically) the number of galaxies resid-

ing in a host halo and assumes that it is governed solely by the halo mass, remaining agnostic about any other halo property. It rests on the long-standing and widely accepted theoretical prediction that halo mass is the attribute that most strongly influences the halo abundance and halo clustering as well as the properties of the galaxies residing in it (White & Rees 1978; Blumenthal et al. 1984). This method provides a framework for “painting” a mock galaxy population on top of large-volume collisionless simulations; i.e. N-body simulations.

The current best approach for probing structure formation on the largest cosmological scales is through N-body simulations. They are vital for making robust predictions for the upcoming galaxy surveys which will cover $\sim \text{Gpc}^3$ volumes (e.g. Euclid and DESI). N-body simulations take substantially less time to evolve compared with hydrodynamical simulations and can therefore be run on sufficiently large volumes. The dark matter halos formed in such a sim-

* E-mail: boryana.hadzhiyska@cfa.harvard.edu

ulations are populated with galaxies according to different recipes, the most ubiquitously used one being the standard HOD formalism (Cooray 2002; Yang et al. 2004; Berlind & Weinberg 2002). While their properties correlate strongly with the parent halo mass, galaxies are known to be biased tracers of the halo and total mass distributions, so other effects need to be taken into account (Norberg et al. 2001; Zehavi et al. 2002). This is known as “galaxy assembly bias”. Numerical simulations have shown that properties such as halo formation time, environment, concentration, triaxiality, spin, and velocity anisotropy play a role in determining the clustering of halos (Gao & White 2007; Wechsler et al. 2006; Dalal et al. 2008; Wang et al. 2009; Lacerna et al. 2014; Wechsler et al. 2006; Faltenbacher & White 2010; Lacerna & Padilla 2012; Abbas & Sheth 2007; Pujol et al. 2017; Paranjape et al. 2018; Shi & Sheth 2018), but whether the properties of the galaxies are correlated with any of these remains an open question (Croton et al. 2007; Beltz-Mohrmann et al. 2019). Should it turn out to be the case, then the standard HOD assumption will be violated, and these models will likely fail to predict the clustering statistics of galaxies correctly to the necessary degree of precision. This failure will be particularly pronounced when trying to create mocks for specially selected galaxy samples (e.g. on the basis of their color or star formation rate).

One way to check whether the modeling for future surveys is done at the required levels of precision is by testing the HOD model against hydrodynamical simulations. Hydrodynamical simulations have now reached a state where they are sufficiently large in volume and high enough in resolution that cosmologists can use them to study the largest structures in our Universe formed by the elusive dark matter component (Dubois et al. 2014; Schaller et al. 2015; Dolag et al. 2016; McCarthy et al. 2017; Springel et al. 2018). These simulations can constrain small-scale physical processes that lead to the formation of galaxies and change their morphology and evolution. In addition, they are invaluable for testing various theoretical models by comparing their outcome to observations in the real universe.

One particular set of cosmological simulations which incorporates state-of-the-art baryonic physics models and is useful for probing the clustering of galaxies (Gao et al. 2005; Gao & White 2007) is provided by the IllustrisTNG (TNG) team (Springel et al. 2018; Pillepich et al. 2018b; Nelson et al. 2018a; Naiman et al. 2018; Marinacci et al. 2018). These models account for a wide range of the physical processes which are believed to govern the formation of galaxies and, therefore, TNG is well-suited to answer a broad range of questions regarding how structure in the Universe evolved over time. In particular, the largest box, TNG300-1 ($L_{\text{box}} = 205 \text{ Mpc}/h$), has sufficient volume and resolution to study clustering of the matter components at relatively large scales ($\sim 20 \text{ Mpc}/h$) (but not sufficiently big to make robust predictions for the upcoming galaxy surveys) and matches well the observed galaxy clustering (Springel et al. 2018).

In this paper, we investigate whether there are significant violations in the mass-only HOD model assumptions and what halo properties have the most significant effect on galaxy clustering according to the TNG model. We will refer to this formulation of the HOD as the “standard” approach from here on. The paper is organized as follows: in Section 2, we discuss the parameters and specifications of the sim-

ulations and group finders we have employed as well as the main algorithm that we follow to test the standard HOD formalism. In Section 3, we present results from our test of the HOD model in TNG300; we then check its statistical robustness via N-body only boxes of comparable volume, using different halo definitions. In Section 4, we investigate which secondary halo properties can explain the discrepancy we have observed. We then develop a straightforward algorithm which allows us to implement an additional partial dependence of the halo occupation number on an extra halo property. We finally concentrate on the environmental dependence and study how the clustering changes when we hold fixed the type of environment. In Section 5, we summarize our results and make elementary proposals for diminishing the effect of galaxy assembly bias on galaxy assignment recipes in N-body simulations.

2 METHODS

2.1 Simulations

In this section, we describe the numerical data used in this work, providing a brief overview of the relevant simulations. Our primary source is the suite of IllustrisTNG hydrodynamic simulations and their dark-matter-only counterparts, as summarized in the TNG data release (Nelson et al. 2019b)¹. We then test the impact of finite box size and cosmic variance in the clustering measured in TNG using a much larger N-body simulation volume.

2.1.1 IllustrisTNG

The Next Generation Illustris simulation (IllustrisTNG), run with the AREPO code (Springel 2010; Weinberger et al. 2019), consists of 9 simulations: 3 box sizes (300, 100 and 50 Mpc on a side), run at 3 different resolutions each (Nelson et al. 2019a; Pillepich et al. 2019). IllustrisTNG differs from its predecessor, Illustris (Vogelsberger et al. 2014a,b; Genel et al. 2014) in that its sub-grid model has been improved to fix a number of shortcomings of the old model: specifically its treatment of AGN feedback, galactic winds and magnetic fields (Pillepich et al. 2018a; Weinberger et al. 2017). In addition, there has been some further development of the numerical implementation concerning the flexibility and hydrodynamical convergence of the code.

In this work, we use the largest box, at its highest resolution, TNG300-1, a periodic cube of size 205 Mpc/h and mass resolution of $5.9 \times 10^7 M_{\odot}$ and $1.1 \times 10^7 M_{\odot}$ for the dark matter and baryons, respectively. We take advantage of the fact that TNG provides both the hydrodynamical (or full-physics, FP) simulation output as well as the dark matter only (or N-body, DMO) one, evolved from the same set of initial conditions. This gives us an opportunity to make a halo-by-halo assignment of galaxies by cross-matching the full-physics and dark-matter-only simulations. The halos (groups) in TNG are found with a standard friends-of-friends (FoF) algorithm with linking length $b = 0.2$ run on the dark matter particles, while the subhalos are identified using the SUBFIND algorithm (Springel et al. 2001), which detects

¹ www.tng-project.org

substructure within the groups and defines locally overdense, self-bound particle groups.

2.1.2 Abacus

We use the publicly released data products produced as part of the AbacusCosmos N-body simulation suite² (Garrison et al. 2018a) to test the statistical robustness of our results, in particular cosmic variance and box-size effects. We work with the halo catalog for a box of size 720 Mpc/h with 1440³ dark matter particles which uses *Planck* 2015 cosmology (Garrison et al. 2018b). ABACUS delivers both high speed and accuracy, as it utilizes novel computational techniques and high performance hardware – e.g. GPUs and RAID disk arrays. The force computations are split into a near-field component, calculated directly, and a far-field component, computed from the multipole moments of particles in the cells. The initial conditions are obtained by scaling back the $z = 0$ power spectrum output from CAMB (Lewis & Challinor 2011) to $z = 49$ and using growth factor ratios. The initial positions and velocities of the particles are then generated through an implementation of 2LPT which includes a rescaling, as the growing modes near k_{Nyquist} are shown to be suppressed due to the fact that the dark matter particles are treated like macroparticles (Garrison et al. 2016). Halos are identified using a nested FoF halo-finding procedure with two linking length values, 0.186 and 0.117.

2.2 Procedure

The main assumption of the standard HOD model used to populate N-body simulations with galaxies is that the number of galaxies residing in a halo depends solely on the mass of that halo. Here we test this conjecture by making use of both the IllustrisTNG dark-matter-only output as well as the full-physics one. Combining these two datasets allows us to draw direct statistical comparisons between the “truth” (defined by the full-physics run) and the HOD model.

Typically, the HOD model has a functional form with several free parameters which determine the average halo occupation number as a function of mass, M . The model assumes that the number of halos is Poisson sampled from a distribution $N(M)$.

Here, we empirically derive the galaxy occupation numbers per halo (HOD) by extracting them from the TNG full-physics simulation. We then populate the dark-matter-only halos by randomly shuffling the galaxy occupation numbers in halo mass bins: this procedure mimics the standard implementation of the basic HOD because it preserves mean occupation number as a function of mass, which is the fundamental assumption of the “basic” HOD.

Throughout the paper, we will be referring back to the prescription outlined below as the shuffling/ordering procedure (see Fig. 1):

1. Bijectively match as many of the halos across the dark-matter-only (DMO) and full-physics (FP) TNG300-1 simulations:

A full-physics subhalo is found to be the bijective match of a dark-matter-only subhalo if they share most of each other’s particles (Lovell et al. 2018; Nelson et al. 2019b). If the central subhalos of a dark-matter-only and a full-physics halo are bijective matches, then their halo parents are also associated through a bijective match.

2. Assign the same number of galaxies to the halos in the dark-matter-only simulation as their corresponding full-physics counterparts (as obtained in 1.) to obtain the **fiducial (unshuffled)** galaxy sample.

To create the second, **shuffled/ordered** sample, instead of assigning the full-physics galaxies to the bijectively matched halos, we split the halos into mass bins such that the fractional change within each bin $\frac{M_{\text{max}} - M_{\text{min}}}{M_{\text{avg}}} \lesssim 5\%$. We have checked that the size of these mass bins is sufficiently small, so the HOD shape is completely preserved upon shuffling/ordering.

2'. Order the halos by mass (keeping track of how many galaxies each would receive from the bijective match) and, within each mass bin, reassign the number of galaxies by either:

- a. randomly shuffling them
- b. ordering them by some halo property (halo concentration, environment, accretion rate).

Note that we exclude the most massive halos (100 in the case of the TNG300-1 box) because the halo mass function contains very few examples of such high-mass systems.

3. The galaxies within a given halo are assigned to the subhalos in order of the subhalos’ V_{peak} (peak magnitude of the circular velocity attained by the subhalo at any point in its evolution); i.e. the subhalos with the highest V_{peak} gets the first galaxy, the second highest gets the second, etc. There are always more subhalos than galaxies that need to be assigned to a given FOF.

4. Split the volume of the simulation into $3^3 = 27$ equal parts and define 27 subsamples by excluding in each a different cube of side $(205/3)$ Mpc/h ≈ 68 Mpc/h from the total volume.

5. Compute the correlation functions of the shuffled/ordered and fiducial (unshuffled) galaxies in each of the 27 subsamples using the Landy-Szalay equation (Landy & Szalay 1993)

$$\hat{\xi}_{\text{LS}}(r) = \frac{DD(r)}{RR(r)} - 1, \quad (1)$$

assuming periodic boundary conditions.

6. To obtain the correlation function and corresponding errors for the full box, calculate the mean and jackknife errors of the correlation functions for the 27 subsamples and their ratios adopting the standard equations

$$\overline{\xi(r)} = \frac{1}{n} \sum_{i=1}^n \overline{\xi(r)}_i \quad (2)$$

$$\text{Var}(\overline{\xi(r)}) = \frac{n-1}{n} \sum_{i=1}^n (\overline{\xi(r)}_i - \overline{\xi(r)})^2, \quad (3)$$

where $n = 27$ and $\overline{\xi(r)}_i$ is the correlation function value at r for subsample i (i.e. excluding the galaxies residing within volume element i in the correlation function computation).

² The data products can be found at <https://lgarrison.github.io/AbacusCosmos/>.

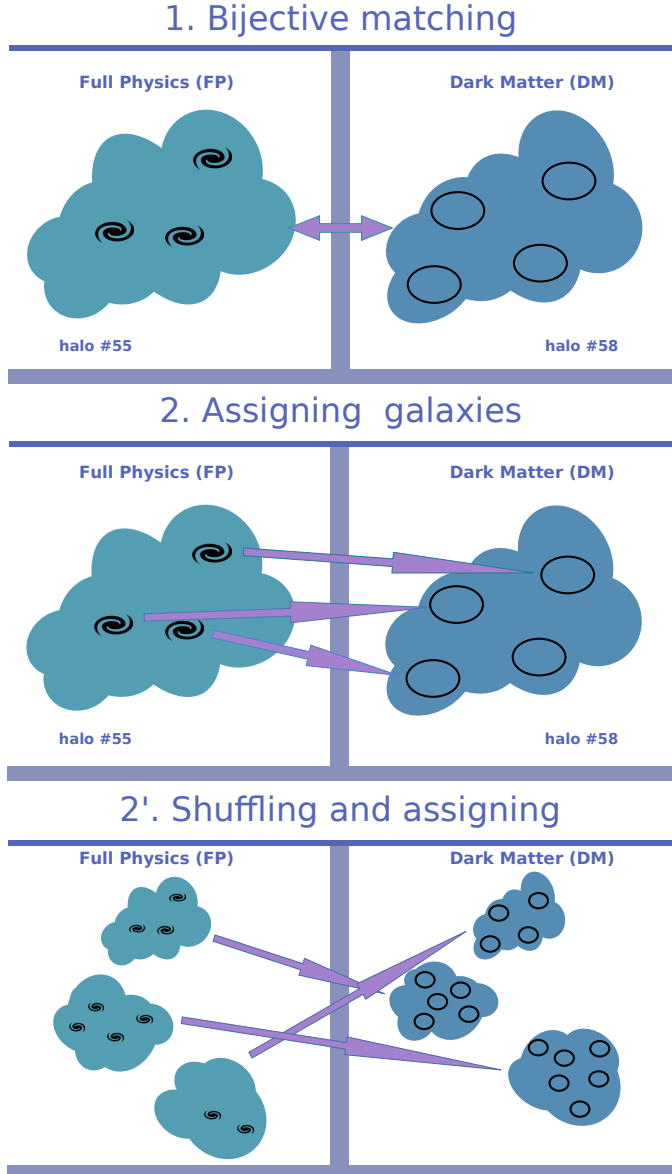


Figure 1. Illustration of the procedure outlined in Section 2.2. In the first step, we match the halos in the full-physics (FP) TNG300-1 simulation (*left*) to those in the dark-matter-only (DM) one (*right*) based on particle IDs. We then have two choices denoted by “2.” and “2'.” respectively. We can either assign the N galaxies that reside in each full-physics halo to the N subhalos with highest V_{peak} in the matched dark-matter-only halo or alternatively, we can assign those N galaxies to a different halo belonging to the same mass bin.

3 BASE MODEL

3.1 Shuffled occupations

To ensure that the galaxy sample from IllustrisTNG is robust, we define our galaxies as subhalos with at least 10,000 gravitationally bound star particles, which results in a galaxy sample with a number density of $n_{\text{gal}} \approx 1.3 \times 10^{-3} [\text{Mpc}/h]^{-3}$. In Fig. 2, we show the HOD derived from full-physics TNG300-1 following the shuffling procedure de-

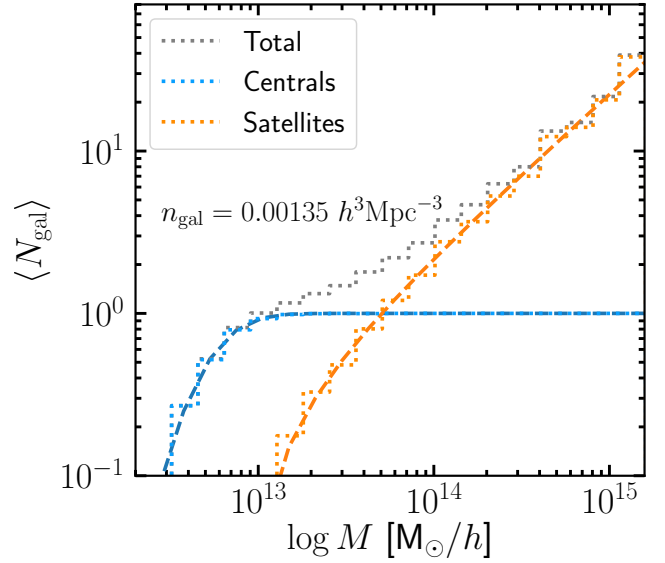


Figure 2. Histogram of the average number of galaxies per halo as a function of halo mass (halo occupation distribution) in TNG300. Here, we use $M_{200\text{m}}$ as the halo mass definition and break the galaxy sample into two populations – centrals and satellites. We also show fits (*dashed line*) to these populations assuming the 5-parameter HOD model described in the text (Zheng et al. 2005).

scribed in Section 2.2. We also fit the 5 basic HOD parameters from Zheng et al. (2005) to describe the central and satellite mean occupation functions

$$\langle N_{\text{cen}}(M_h) \rangle = \frac{1}{2} \left[1 + \text{erf} \left(\frac{\log M_h - \log M_{\text{min}}}{\sigma_{\log M}} \right) \right] \quad (4)$$

and

$$\langle N_{\text{sat}}(M_h) \rangle = \left(\frac{M_h - M_{\text{cut}}}{M_1} \right)^\alpha, \quad (5)$$

where M_{min} is the characteristic minimum mass of halos that host central galaxies, $\sigma_{\log M}$ is the width of this transition, M_{cut} is the characteristic cut-off scale for hosting satellites, M_1 is a normalization factor, and α is the power-law slope. Our halo mass proxy is $M_h = M_{200\text{m}}$, which is the total mass within a sphere with mean density 200 times the mean density of the Universe. Fig. 2 demonstrates that Eqs. 4 and 5 capture the overall shape of the HOD from our simulations very well. The corresponding values for the 5 free parameters of this model are: $\log M_{\text{min}} = 12.712$, $\sigma_{\log M} = 0.287$, $\log M_{\text{cut}} = 12.95$, $\log M_1 = 13.62$ and $\alpha = 0.98$.

Fig. 2 remains unchanged after performing a shuffling of the occupation numbers in 5% mass bins following the recipe outlined in Section 2.2. In other words, if the only relevant property to large-scale galaxy clustering is halo mass, then the galaxy-galaxy correlation functions in the shuffled and the unshuffled cases should be statistically consistent on large scales, and any deviations are suggestive of violations of some of our assumptions.

The top panel of Fig. 3 shows the correlation function of the “true” galaxy distribution in the full-physics simulation run of TNG300-1 in orange, the bijectively matched ones in

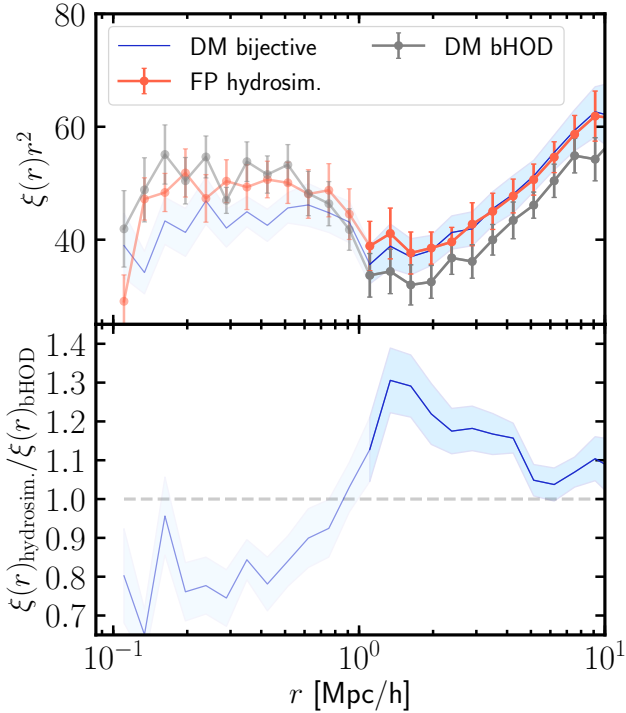


Figure 3. Correlation functions of the full-physics galaxies (FP hydrosim.), the bijective matches (DM bijective), and those shuffled in 5% bins (DM bHOD) (*upper panel*). The ratio of bijectively matched to shuffled (*lower panel*) shows a big discrepancy on large scales of 15%, which should not exist if mass is the only halo property that determines the average halo occupation. All errors are jackknife. This 15% deviation persists even if we relax the definition of a galaxy from a subhalo containing at least 10000 bound star particles to one containing at least 5000.

blue and the shuffled case, i.e. mimicking the HOD model, in gray. The bottom plot shows the ratio between the blue and gray curves. The proxy used for halo mass here is M_{200m} .

Fig. 3 shows that the clustering of the full-physics galaxies on scales above 1 Mpc/h is substantially larger, 10–30%, than those of the shuffled dark matter. This is the key result of our paper, as it indicates a clear violation of the assumptions of the basic HOD model. We evaluate this discrepancy by averaging the percentage difference for $20 \text{ Mpc}/h > r > 1 \text{ Mpc}/h$ and find it to be $15 \pm 1\%$ (accounting for the random variation when shuffling). In the subsequent sections, we will attempt to determine the cause of this difference as well as subject it to more rigorous testing. The difference between bijectively matched curve (blue) and the full-physics curve (orange) on scales below $r \leq 1 \text{ Mpc}/h$ is purely a consequence of how we choose to populate the central and satellite galaxies within the halo which is not a subject of study in this paper. We therefore attribute no particular importance to the differences on such scales.

3.2 Choice of halo finder

An often overlooked potential source of discrepancy in N-body simulations, apart from the lack of baryonic physics,

is the implementation of halo-finding algorithms, which aim to identify bound structures (halos) using information about the distribution of particles in the simulation over time or at a particular snapshot. A very commonly used and relatively fast approach employs the friends-of-friends (FoF) algorithm, which links together all particles whose mutual separation is less than the so called linking length parameter, b . A problem with the FoF algorithm is ‘percolation’, in which many fragmented objects can be linked together as one, resulting in unphysical objects entering the halo catalog. This pathology could have an impact on statistical properties like halo abundance and clustering. Furthermore, it can bias weak-lensing estimates of cluster masses at a level comparable to the precision of the most advanced experiments and lead to differences in e.g. the halo mass function beyond the few percent precision necessary for cluster abundance experiments such as SDSS, DES, DESI, Euclid, and LSST (Garcia & Rozo 2019). We are interested in the effect of the FoF algorithm on the galaxy clustering in TNG, as the choice of linking length can result in different structures being linked together (or not), and might therefore affect the dark-matter-only and full-physics halo catalogs differently due to chance fragmentations.

Algorithms that identify halos or analyze the particle trajectories using full 6D phase-space information (i.e. positions and velocities) such as ROCKSTAR and SPARTA may be better at circumventing these halo pathologies. They are typically run in post-processing and can provide alternative halo catalogs to standard on-the-fly implementations. One can conjecture that the observed discrepancy on large scales in Fig. 3 is due to the FoF catalog, containing an excess of smaller halos on the outskirts of larger groups if the linking length is too small. Then, as we reshuffle, we place galaxies in halos which should have been part of other larger halos, whose mass has been undermined due to this effect of overshredding. This results in a suppression of the correlation function on large scales.

To test this conjecture, we run ROCKSTAR, a phase-space, temporal halo finder (Behroozi et al. 2013a), on the final state ($z = 0$) of the TNG300-1-Dark box. In Fig. 4, we show the cross-correlation between the 400 most massive and the 500,000 most massive parent halos in both the (spatial-only) FoF and the ROCKSTAR halo catalogs (effectively a phase-space FoF finder), using M_{200m} and the virial mass M_{vir} , respectively, as defined by each catalog. Contrary to our expectation, we find an excess of halos separated by $\sim 1 \text{ Mpc}/h$ in the ROCKSTAR catalog relative to the FoF one (which we also observed for different mass-scale choices of the two sets of halos being cross-correlated). This suggests that there is *less* overshredding in the FoF halo sample with ROCKSTAR tending to find more satellite halos orbiting at the outskirts of larger halos than FoF. Indeed, as Table 1 suggests, the use of the ROCKSTAR catalog does not alleviate the discrepancy illustrated in Fig. 3, and we still find a difference on large scales of order 15%.

Another possible source of error is the definition of halo mass. It has been proposed (Diemer & Kravtsov 2014; Adhikari et al. 2014; More et al. 2015; Diemer 2017) that a more physical definition of a halo boundary is the ‘splash-back radius’, defined as the apocenter of all particles that ever fall into the potential well of what is ultimately defined as the halo. We have compared the TNG FoF catalog with

one augmented with SPARTA, an algorithm designed for computing splashback radii, and have confirmed that the TNG FoF catalog provides a value for M_{200m} comparable to the splashback mass, $M_{sp} \lesssim 2M_{200m}$, obtained by Diemer (2017), in the mass range of our interest at $z = 0.1$ (see also Fig. 3 in Diemer et al. (2017) which shows a similarity between the masses and radii at $z = 0$). The scatter in the relation between M_{sp} and M_{200m} depends prominently on the accretion rate of halos which is directly related to the halo clustering. Despite the similarity between M_{200m} and M_{sp} , we would need to test more robustly the conjecture that using either as a mass proxy in the HOD model would lead to equivalent results in the case of TNG300 (Mansfield & Kravtsov 2019).

We explore other popular mass definitions such as M_{200c} and V_{peak} . The procedure for reshuffling is the same as outlined in Section 2.2, the only difference being the mass proxy used for creating the 5% mass bins. The results, shown in Table 1, indicate that indeed defining halo mass as M_{200m} leads to the least amount of discrepancy on large scales ($r = 1 - 20$ Mpc/h), of $12 \pm 1\%$, out of the commonly used mass proxies.

Out of all definitions, the discrepancy is smallest, $8 \pm 1\%$, when we adopt M_{FoF} . We believe that this is most likely due to the play of several different FoF properties. In particular, we point out the tendency of the FoF algorithm to join together several subhalos which may not be gravitationally bound to the cluster but are located in close proximity to it. In this way, the correlation between halo mass M_{FoF} and number of satellites is strengthened and our reordering using M_{FoF} becomes effectively a reordering on the number of satellites, which by construction increases the clustering of satellite galaxies (Pujol & Gaztañaga 2014). This result can be interpreted either as an indication that the halo structure extends beyond the conventional spherical radius of R_{200m} for some objects or as an indication of possible anomalies with the FoF algorithm.

3.3 Checking box-size effects and cosmic variance with Abacus

Some of the main concerns regarding the robustness of our results are the limited size of the TNG box and the cosmic variance, which may play a significant role on the scales considered. To test whether that is the case, we repeat the procedure from Section 2.2 of shuffling the halo occupations in 5%-mass bins, but this time using a multitude of N-body simulation boxes of similar size and resolution to TNG300-1 (27 in total). To this end, we select an initial Poisson draw from the HOD distribution for each of the 27 boxes to be the “true” galaxy distribution and then apply the shuffling procedure. We finally examine the scatter in all 27 boxes in an effort to better quantify the statistical significance of our TNG results. The cosmic variance check also helps quantify whether TNG300 is simply an abnormal region of space where the HOD fails as a statistical fluctuation, rather than a physical effect.

Here is the recipe in more detail:

1. Numerically derive the average number of galaxies per halo as a function of the halo mass measured in logarithmic bins from the TNG300-1 full-physics simulation box, i.e. the histogram in Fig. 2.
2. Make a Poisson draw for each ROCKSTAR or FoF halo

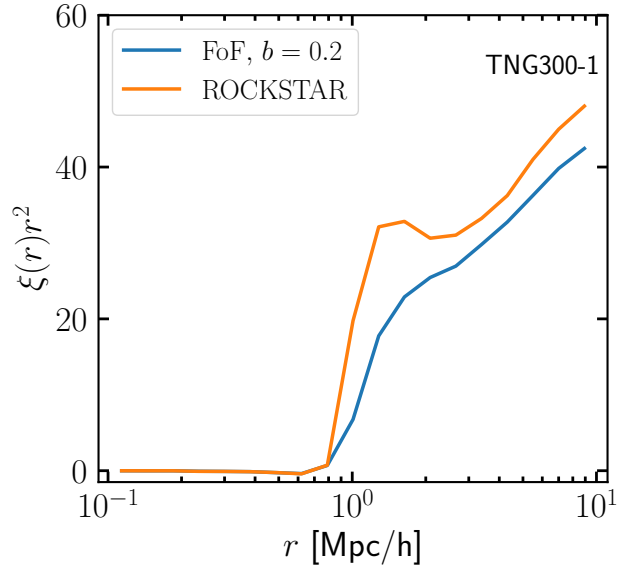


Figure 4. Cross correlation between the 400 most massive and the 500,000 most massive halos in TNG300-1-Dark as defined by ROCKSTAR and FoF with linking length $b = 0.2$. For a mass proxy we use M_{200m} . The bump around $r = 1$ Mpc/h shows that there are more intermediate-size halos found near the boundaries of the largest halos in the ROCKSTAR case compared with the FoF.

in the ABACUS $L_{box} = 720$ Mpc/h box to obtain the number of galaxies it contains. (We use both halo catalogs for consistency checking.)

3. Evaluate the galaxy number density and if necessary renormalize the halo masses in ABACUS (multiplying them by a $\mathcal{O}(1)$ factor) until the galaxy number densities between TNG300-1-Dark and ABACUS match.

4. Split the ABACUS box into 27 cubic subboxes of length $L_{box} = \frac{1}{3}720$ Mpc/h = 240 Mpc/h. The size of each subbox is now comparable to that of TNG300, $L_{box} = 205$ Mpc/h.

5. For each of the 27 subboxes, we repeat the steps in Section 2.2 with mass proxy M_{200m} , as before. The only difference is that within the halo boundaries, we place the central galaxy and its satellites inside the dark-matter halo, so that their positions trace the best-fitting NFW profile (Navarro et al. 1996, 1997) that quantifies the DM distribution in these halos. This choice does not affect the galaxy clustering results on large scales. The subboxes do not have periodic boundary conditions, so we compute the correlation function using

$$\hat{\xi}_{LS}(r) = \left(\frac{N_{rand}}{N_{data}} \right)^2 \frac{DD(r)}{RR(r)} - 2 \frac{N_{rand}}{N_{data}} \frac{DR(r)}{RR(r)} + 1 \quad (6)$$

with $N_{rand} = 35 N_{data}$ random points (Landy & Szalay 1993).

The results are shown in Fig. 5. We see that the mean ratio curve of all 27 ABACUS subboxes differs by only 0.3% from 1 on the scales we are interested in, 1 Mpc/h $< r < 10$ Mpc/h, which is consistent with what would be expected if one randomly shuffles Poisson samples drawn from the same mean distribution. This is effectively what we do when we shuffle the galaxy occupation numbers in 5% mass bins, as the mean HOD is roughly constant for such small mass

Mass proxy	Mass proxy definition used in bHOD	Compared against	Difference from bHOD
M_{200m}	The total mass enclosed in a sphere with mean density 200 times the mean density of the Universe	hydrosimulation	$15 \pm 1\%$
M_{vir}	Total particle mass (within the virial radius) in ROCKSTAR	hydrosimulation	$15 \pm 1\%$
M_{200c}	Total Mass enclosed in a sphere with mean density 200 times the critical density of the Universe	hydrosimulation	$19 \pm 1\%$
M_{500c}	Total Mass enclosed in a sphere with mean density 500 times the critical density of the Universe	hydrosimulation	$19 \pm 1\%$
$\sigma^2 R_{halfmass}$	Dispersion velocity times the radius containing half of the total mass of the largest subhalo	hydrosimulation	$20 \pm 1\%$
V_{peak}	Maximum value of the velocity in a spherically-averaged rotation curve ever achieved by the largest subhalo	hydrosimulation	$20 \pm 1\%$
V_{max}	Maximum value of the velocity in a spherically-averaged rotation curve for the largest subhalo	hydrosimulation	$20 \pm 1\%$
M_{FoF}	Sum of the individual masses of every particle in this group	hydrosimulation	$8 \pm 1\%$

Table 1. Percentage difference between the correlation function of the galaxies assigned in TNG300-1-Dark using the hydrodynamical simulation outputs and the “basic” HOD (bHOD) prescription averaged over the scales $r = 1 - 20$ Mpc/h for different proxies of the host halo mass. The uncertainty we report comes from the fact that we shuffle the data randomly, so each realization offers a slightly different shape of the correlation function. We estimate it as the standard deviation around the mean for ~ 10 random realizations. Fortunately, the scatter is small and does not change the overall conclusions.

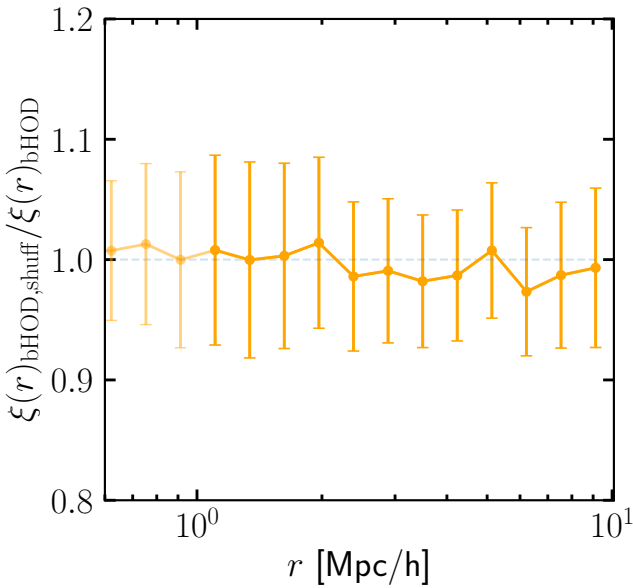


Figure 5. Correlation function ratio between the randomly shuffled basic model assigned halo occupations (bHOD) and the fiducial (unshuffled) case in 27 ABACUS subboxes with $L_{box} = 240\text{Mpc}/h$. In contrast with the TNG300-1 case where we see a discrepancy of 15% on large scales, the ratio in the ABACUS case is consistent with 1 on all scales (differs from 1 at 0.3% for $r > 1$ Mpc/h). Since we cannot mimic the statistical significance of the TNG300-1 result with a simple HOD model, other factors such as assembly bias and baryonic feedback might be at play in the TNG300-1 case. The results we obtain using the FoF-defined halos do not differ significantly from the case of the ROCKSTAR-defined halos.

changes. The standard deviation is 6.0%, which is smaller than the observed average 10-20% deviation in the case of TNG300-1 (Table 1). This gives us confidence the TNG result shown in Fig. 5 is not a manifestation of cosmic variance or box-size effects.

4 THE SEARCH FOR A SECOND PARAMETER

In this section, we explore which secondary properties of the halo have the strongest effect on the large-scale clustering of galaxies. Previous analyses have suggested that, in addition to halo mass, the overdensity in which the halo resides and the concentration of its DM density profile may also play defining roles in setting the galaxy bias (Zehavi et al. 2018; Artale et al. 2018; Bose et al. 2019). Other properties such as halo spin and accretion rate history have been shown to be either of tertiary importance or strongly correlated with the halo concentration.

4.1 Candidates for secondary parameter

To investigate the extent to which secondary properties affect the galaxy clustering on large scales, we run a simple test. We again apply the procedure in Section 2.2 to TNG300-1, but instead of randomly shuffling the halo occupation numbers, we assign the galaxy number to each halo within the given 5% mass bin in order of decreasing or increasing value of the secondary halo property (i.e. 2’b) in the procedure).

4.1.1 Local environment

The effect of environment on the halo and galaxy clustering has been studied extensively in the literature (Abbas & Sheth 2007; Pujol et al. 2017; Paranjape et al. 2018; Shi & Sheth 2018). A halo residing in a dense region is expected to contain more galaxies on average than a halo in an underdense region. This is because halos in overdense regions experience more mergers, whereas those in underdense regions have more mass accreted in the form of smooth material. To assess the extent to which local environment affects the large-scale clustering, we adopt the following definition for “environment factor” for each halo:

1. Count the number of subhalos (as defined via the

SUBFIND algorithm (Springel et al. 2001)) in a radius of $R_{\text{tot env}} = 5 \text{ Mpc}/h$ centered on the halo centre and sum up their masses, $M_{\text{tot env}}$.

2. Count the number of subhalos in a radius of R_{200c} and sum up their masses, $M_{200c \text{ env}}$.

3. Subtract the mass within the 200 critical radius from the total mass contained in the halo environment and obtain the mass of the environment, $M_{\text{env}} = M_{\text{tot env}} - M_{200c \text{ env}}$.

4. Normalize by the average environment mass of all halos in the HOD and define the environment factor, $f_{\text{env}} \equiv M_{\text{env}}/\bar{M}_{\text{env}}$.

Ordering the halo occupation number within each 5% mass bin in order of largest to smallest environment factor, f_{env} , we compute the correlation function and compare it with the fiducial case. We see a strong bump near $r \approx 5\text{Mpc}/h$ in the second top panel of Fig. 6 I which suggests that environment might play a more crucial role in determining the clustering of galaxies on large scales than expected. An important caveat in the environment parameter definition is that we condition on exactly the galaxies that will be counted in the correlation function, i.e. those separated by $\sim 5 \text{ Mpc}/h$. We explore this parameter further in Section 4.3.

4.1.2 Mass measure assuming virial theorem

According to the virial theorem, the mass of a bound object can be estimated from

$$\frac{GM_{\text{vir}}}{R_{\text{vir}}} = \sigma^2, \quad (7)$$

where σ is the velocity dispersion. Thus, for a virialized structure, the combination of $\sigma^2 R_{\text{vir}}$ may be interpreted as an excellent mass proxy. However, this rests on the assumption that the FoF halos of TNG300 are virialized structures and that is unlikely to apply to all particles belonging to the edges of a large halo.

The most widely accepted choice for a virialized mass proxy is M_{200m} , but there are many other mass proxies which can be used, none of which are perfect. Here we condition on a second mass proxy, the combination $\sigma^2 R_{\text{halfmass}}$. We use the velocity dispersion σ of the most massive subhalo (identified through SUBFIND) in the given halo, and the halfmass radius R_{halfmass} of again the most massive subhalo. This quantity could capture the mass of the largest bound structure of the halo through its dynamical behavior.

The TNG halo catalog reveals a strong correlation between conventional halo mass proxies such as M_{200m} and the combination $\sigma^2 R_{\text{halfmass}}$. We first attempt to use this parameter as mass proxy and apply a random shuffling in 5% mass bins. From Table 1 we learn that it is not as effective as some of the other mass proxies (e.g. M_{200m}). We next condition on $\sigma^2 R_{\text{halfmass}}$ as a secondary parameter, ordering it in reverse so that halos with smaller values of $\sigma^2 R_{\text{halfmass}}$ become hosts to a larger number of galaxies. The motivation for doing so is that the velocity dispersion is expected to have an inverse relationship with halo occupation at fixed mass (Bose et al. 2019) and a smaller half-mass radius of the central galaxy might be indicative of a galaxy cluster where the satellites have not been accreted onto the central galaxy. Intriguingly, the result in Fig. 6 II indicates that indeed we get very strong large-scale correlation when we condition on

this combination of parameters. This suggests that dynamical descriptions of the halo are likely to tie more directly to its merger history and thus to the expected number of the galaxies it is hosting. A possible explanation is that similarly to the velocity dispersion, $\sigma^2 R_{\text{halfmass}}$ is related to concentration (i.e. the central density) of the halo, which is correlated strongly with halo occupancy (see Section 4.1.5). The additional effect from R_{halfmass} would be that the larger the central subhalo (in radius), the more likely it is to have consumed the smaller subhalos surrounding it, which suggests that there are more satellite galaxies on average for an object with a small value of $\sigma^2 R_{\text{halfmass}}$. Each of these effects can, in turn, shift the clustering relative to the case where halo occupancy is defined by halo mass only.

Furthermore, we explored a few other related parameters such as $M_{\text{cent}}/R_{\text{halfmass}}$ as a measure of the potential depth and $M_{\text{cent}}/(\sigma^2 R_{\text{halfmass}})$ as a measure of the extent to which halos are virialized, which resulted in a 3% and a 0.2% increase of the large-scale correlation function with respect to the “basic” HOD model (i.e. in the direction of the hydrodynamical simulation), respectively.

4.1.3 Velocity anisotropy

In Jeans’ modeling (Merritt 1987), there is a well-known degeneracy between the mass profile of a distribution of particles and the velocity anisotropy of orbits that trace the resulting potential. This is known as the “mass-anisotropy degeneracy”. The velocity anisotropy is defined as (Binney & Tremaine 1987)

$$\beta = 1 - \frac{\sigma_{\text{tan}}^2}{2\sigma_{\text{rad}}^2}, \quad (8)$$

where σ_{tan} and σ_{rad} are the tangential and radial velocity dispersions, respectively. We calculate these quantities over all particles in the FoF halo by projecting the velocity of each particle along and perpendicular to the radial direction (defined with respect to the position of the particle with the minimum gravitational potential energy) and then computing the standard deviation of each component (Ramakrishnan et al. 2019). It is important to realize that β depends on the shape of the halo, so, similarly to the 3D dispersion, it captures information from the full phase-space structure of the parent halo. The limits of this parameter, $-\infty$ and 1, correspond to radially and tangentially dominated velocity dispersions, respectively, while $\beta = 0$ indicates an isotropic distribution of particle orbits.

Previous works have shown that halos with a high value of β cluster more weakly than those with low β (Faltenbacher & White 2010; Ramakrishnan et al. 2019). For our reordering test, we therefore assign higher number of galaxies to halos with smaller dispersion anisotropy, analogously to how we treat next the velocity dispersion as a secondary parameter. The net effect of this can be seen in Fig. 6 III, which shows a significant increase of the galaxy clustering when comparing it with the true galaxy clustering on large scales. If we quantify this difference, we see that on average this result overshoots the “basic” HOD by about 36% on large scales. In our parameter search, the velocity anisotropy, β is the second most influential secondary parameter on the clustering of galaxies, after local environment (see Table 2).

One plausible explanation for the more isotropic velocity distribution (low value of β) of the more clustered halos (and galaxies) is that the impact parameters of the merging subhalos are larger due to deflections caused by gravity shortly before accretion, hence σ_{tan} acquires a larger value. Since mergers are what dominates the mass growth of halos in high density (i.e. more clustered) regions (Fakhouri & Ma 2009, 2010), they may be influential in determining the velocity structure of these halos and are thus closely related to the number of subhalos (and galaxies) residing in them. As for lower density regions, accretion occurs in a more radial fashion since the gravitational field is dominated by the largest subhalo. This leaves an imprint on the velocity structure of the halo and the value of β increases (Fakhouri & Ma 2009; Faltenbacher & White 2010).

4.1.4 Velocity Dispersion

Similarly to halo concentration (discussed next), the velocity dispersion σ , is correlated with accretion history. However, contrary to the halo concentration, it might be a more directly correlated measure of the most recent merger history of the halo as it uses dynamical information regarding particle velocities rather than simply their positions. Using the TNG simulations, it has been shown that velocity dispersion has an inverse relationship with halo occupation at fixed mass (Bose et al. 2019). For this reason, when applying the reordering procedure outlined in Section 2.2, we give highest priority to the halos with smallest dispersion velocity. We present this result in Fig. 6 IV, which shows a moderate increase of the clustering of HOD galaxies ordered in terms of their velocity dispersion when comparing it with the true galaxy clustering on large scales. If we quantify this difference, we see that on average this result overshoots the “basic” HOD by 18% on large scales. This is the fourth most influential secondary parameter on the clustering of galaxies (see Table 2).

4.1.5 Halo concentration

The concentration of the halo is closely related to its accretion and formation history and has been well studied in the literature (Navarro et al. 1997; Wechsler et al. 2002; Ludlow et al. 2014, 2016). In simplified terms, the larger the number of recent mergers it has undergone, the more spatially spread out its subhalos are likely to be; i.e. the smaller its concentration will be (Bose et al. 2019). A larger number of satellites might imply that halos of smaller concentration have more highly clustered galaxies than the more compact ones. Another important consideration, however, is that as we get to smaller halo masses, where on average we expect 1 or 0 galaxies (i.e. only a central), more concentrated halos are more likely to host a galaxy potentially because the gravitational well is deeper, so gas is more likely to collapse towards the center and form stars. In addition, its dependence on halo mass and environment has also been thoroughly explored (Bullock et al. 2001a; Ludlow et al. 2014; Diemer & Kravtsov 2015). We include it as a likely candidate for assembly bias affecting galaxy clustering and employ the following proxy for halo concentration,

$$c = R_{200c}/R_{\text{max}}, \quad (9)$$

where R_{max} is the radius at which the maximum circular velocity is attained.

We implement the dependence on halo concentration by splitting the halos in two groups depending on their mass: if their mass is larger than some threshold value, M^* , which we define as $\langle N_{\text{gal}}(M^*) \rangle = 1$, we reorder the halo occupation numbers within each 5% mass bin, starting with the least concentrated halos. If, however, the halos within the mass bin have masses smaller than M^* , then we give priority, i.e. grant a central galaxy, to the more concentrated ones. The result is shown in Table 2 and Fig. 6 V. Although we see an improvement of about 3% compared with the random shuffling case, the galaxy clustering on large scales is still not recovered at a sufficient precision for future experiments and a 9% discrepancy remains. This suggests that halo concentration, on its own, is not an effective secondary parameter with which to augment the “basic” HOD model, being less influential than environment and velocity anisotropy in altering the large-scale clustering of galaxies.

4.1.6 Formation Epoch

The characteristic formation epoch of a halo is a direct indicator of its past accretion history at fixed present-day mass. Here, we define formation epoch as the epoch at which the halo has acquired 50% of its present-day mass (using the TNG merger trees (Nelson et al. 2019b)), early-forming halos are expected to have had more time to accrete galaxies due to an expected larger number of mergers and also have, on average, deeper potentials (i.e. early-forming halos are more concentrated). However, the formation epoch (as it is defined here) informs us about the ancient history of the halo and is not as sensitive to the most recent merger events it has undergone, nor is it necessarily correlated with the age of the galaxies residing within it. Even so, many of the early-formed galaxies have consumed their satellites, so modeling the relationship between occupation number and epoch of formation is not an easy task. This is in fact what we find in Table 2 and Fig. 6 VI. Formation history, defined in the way described above, seems to be the weakest assembly bias candidate. It is possible that a definition of formation epoch, spanning over a longer time range or reflective of more recent merger events, might have a more substantial effect on galaxy clustering on the scales of our interest. In particular, a definition that captures both ancient and more recent formation events may be more influential as a secondary parameter with which to augment the “basic” HOD; we leave the exploration of such a metric to future work.

4.1.7 Spin

The final secondary parameter we explore in this section is halo spin. This provides a measure of the angular momentum acquired by the halo and its dependence on other halo properties has been well studied (Bullock et al. 2001b; Bett et al. 2007; Rodríguez-Puebla et al. 2016; Johnson et al. 2019). The measurement of this parameter turns out to be quite sensitive to the particle resolution (the smaller the number of particles in a halo, the larger the error, Oñorbe et al. 2014; Benson 2017).

We adopt the following definition of dimensionless spin

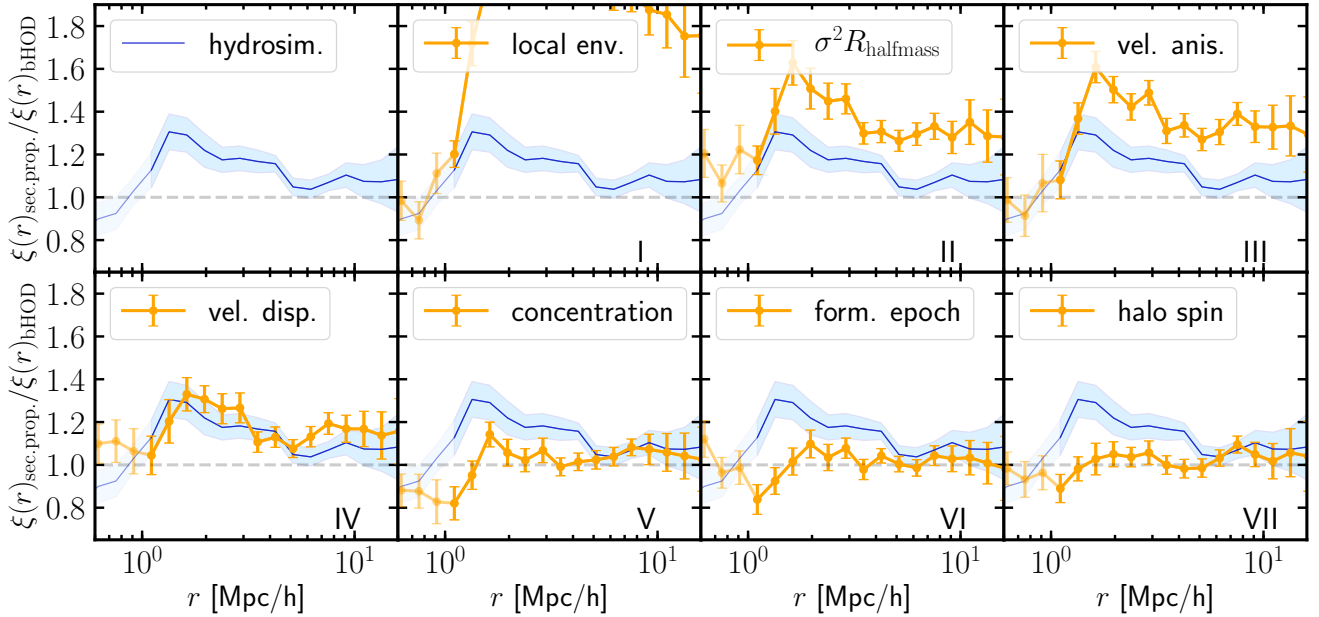


Figure 6. Ratio between the correlation function of the galaxies assigned in TNG300-1-Dark and those in the “basic” HOD (bHOD) prescription. The assignment is accomplished by conditioning on different secondary halo parameters and reordering the halo occupation numbers in 5% mass bins. The secondary parameters considered are the environment factor f_{env} , the dynamical virial mass $\sigma^2 R_{\text{halfmass}}$, the velocity anisotropy β , the velocity dispersion σ , halo concentration c , the formation epoch, and the halo spin λ , always shown in orange (left to right, top to bottom). In shaded blue we show the result from the bijective match between the halos in the full-physics TNG300-1 box and the dark-matter-only TNG300-1 box. The mass proxy used in all cases is $M_{200\text{m}}$.

λ proposed by Bullock et al. (2001b)

$$\lambda = \frac{J_{\text{vir}}}{\sqrt{2} M_{\text{vir}} R_{\text{vir}} V_{\text{vir}}}, \quad (10)$$

where J_{vir} is the angular momentum inside a sphere of radius R_{vir} of mass M_{vir} and with halo circular velocity $V_{\text{vir}} = \sqrt{GM_{\text{vir}}/R_{\text{vir}}}$. Since we only consider subhalos comprised of ≥ 10000 star particles as galaxies, the sample of halos for which we compute the spin are predominantly $\log M \gtrsim 12.7$, and are sufficiently well-resolved so that noisy spin measurements are not an issue (Benson 2017).

In Table 2 and Fig. 6 VII, we show the resulting percentage difference. It shows a moderate improvement of about 2% with respect to the randomly shuffled case when we preferentially give the largest number of galaxies to the halos with largest spin (or in this case, λ). Hence, we can conclude from this analysis that halo spin plays a minor role in predicting the occupation number of a halo.

4.2 Predicting the correlation function shape

In Section 4, we showed that the parameters that are most influential in shifting the large-scale clustering in the direction of the hydrosimulation result are the local environment parameter f_{env} , the velocity anisotropy β , and the dynamical mass proxy $\sigma^2 R_{\text{halfmass}}$. We did this by a perfect association of ranks between the halo occupation and the second parameter (e.g. the halo with the largest value of f_{env} gets assigned the largest number of galaxies in each 5% mass bin). If one wants to consider an imperfect association which recovers the clustering of galaxies in TNG, one needs to introduce a

new procedure that preserves the original distribution of the occupancies.

In the spirit of our random-shuffling approach, we apply the following procedure which attempts to quantify the strength of this correlation. For each 5%-mass bin with N_{h} halos in it:

1. We choose a correlation parameter r between 0 and 1 and draw N_{h} pairs of (x, y) values from a joint Gaussian distribution with mean $(0, 0)$ and covariance matrix $[[1, r], [r, 1]]$.
2. We convert the (x, y) array into an array of integers by ordering the x -values from largest to smallest, each one getting a number from 0 to $N_{\text{h}} - 1$, respectively. We repeat this for the y -values, obtaining N_{h} pairs of integers, $(x, y) \rightarrow (i, j)$.
3. We now form an array of N_{h} , each entry of which containing the number of galaxies hosted by a halo, N_{gal} , and order it from largest to smallest.
4. We convert them to integers i_{par} between 0 and $N_{\text{h}} - 1$ as before. Similarly, we create another array filled with the values of whichever secondary parameter we are exploring – f_{env} , $\sigma^2 R_{\text{halfmass}}$, or β , and again convert them into an integer array j_{par} .
5. Order the (i, j) pairs in order of the i values and do the same for the array of i_{par} values. Identifying the i 's with the i_{par} 's, we now know what the corresponding j value is for each i_{par} .
6. Find the original value of the $j_{\text{par}}^{\text{th}}$ parameter in the secondary property array for each element i (or equivalently i_{par}) in the pair (i, j) , for which $j = j_{\text{par}}$. We thus effectively end up with a uniform distribution of discrete correlated

Mass proxy	Secondary property	Secondary property definition used in bHOD	Difference from bHOD
M_{200m}	hydrosimulation	Hydrosimulation results from TNG300-1 for the galaxy distribution	$15 \pm 1\%$
M_{200m}	local environment	f_{env} , mean density in an annulus of R_{200m} to $R_{\text{tot env}} = 5 \text{ Mpc}/h$ surrounding the halo	98.6%
M_{200m}	$\sigma^2 R_{\text{halfmass}}$	Dispersion velocity times the radius containing half of the total mass of the largest subhalo	35.4%
M_{200m}	velocity anisotropy	$\beta = 1 - \sigma_{\text{rad}}^2 / 2\sigma_{\text{tan}}^2$ of the largest subhalo (σ_{rad} , σ_{tan} are tangential and radial dispersion)	35.8%
M_{200m}	dispersion velocity	σ , one-dimensional velocity dispersion of all the member particles of the largest subhalo	17.9%
M_{200m}	$M_{\text{cent}}/R_{\text{halfmass}}$	Mass of the largest subhalo divided by the radius containing half of its total mass	6.1%
M_{200m}	halo concentration	$c = R_{200c}/R_{\text{max}}$ (R_{max} is the comoving radius where V_{max} of the largest subhalo is achieved)	2.7%
M_{200m}	halo spin	$\lambda = J_{\text{cent}}/\sqrt{2}M_{200m}R_{200m}V_{200m}$ (J_{cent} is total angular momentum of the largest subhalo)	2.0%
M_{200m}	formation epoch	Snapshot during which the largest subhalo acquired half of its total present mass	0.6%

Table 2. Percentage difference between the correlation function of the galaxies assigned in TNG300-1-Dark using the hydrodynamical simulation outputs conditioned on different secondary halo parameters and the “basic” HOD (bHOD) prescription averaged over the scales $r = 1 - 20 \text{ Mpc}/h$. The most influential assembly bias parameters seem to be environment followed by the virial-mass-like combination $\sigma^2 R_{\text{halfmass}}$ and the halo velocity anisotropy.

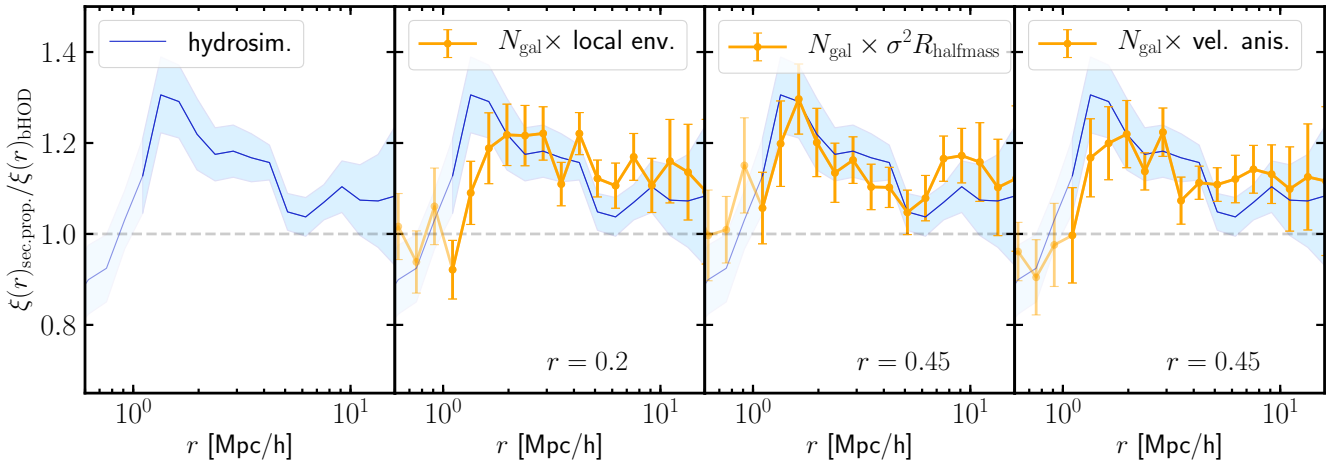


Figure 7. Ratio between the correlation function of the galaxies assigned in TNG300-1-Dark and those in the “basic” HOD (bHOD) prescription. The halo occupation numbers are reordered in 5% mass bins according to the strength of the co-dependence between a given secondary halo parameter and the number of galaxies hosted by the host halo. The recipe is specified in Section 4.2. The secondary parameters considered are the environment factor f_{env} , the dynamical virial mass $\sigma^2 R_{\text{halfmass}}$, and the velocity anisotropy β , always shown in orange (left to right) with the following correlation parameters r : $r = 0.2$, $r = 0.45$ and $r = 0.45$, respectively. The r values are chosen so as to minimize the fractional difference of the galaxy correlation function with respect to the hydrosimulation on large scales ($1 \text{ Mpc}/h < r < 20 \text{ Mpc}/h$). In shaded blue we show the result from the bijective match between the halos in the full-physics TNG300-1 box and the dark-matter-only TNG300-1 box. The mass proxy used in all cases is M_{200m} .

pairs, e.g. a Gaussian drawn ($N_{\text{gal}}, f_{\text{env}}$) distribution, for a given choice of the correlation parameter r .

The amount of correlation, r , between the number of galaxies per halo and one of the three parameters, f_{env} , β , and $\sigma^2 R_{\text{halfmass}}$, which is required to obtain approximately the same behavior of the correlation function on large scales for each of the three parameters as in the hydrosimulation, is $r = 0.2$, $r = 0.45$ and $r = 0.45$, respectively. In Fig. 7, we

show what the resulting correlation functions look like in adopting these values for the correlation parameter r .

4.3 The environment factor

As was shown in Table 2 and Fig. 6 I, the biggest impact on the clustering of galaxies on large scales after halo mass is the environment. In this section, we explore other, more

rigorous definitions of the environment parameter than the one used previously – in particular, we quantify a halo’s tidal environment, and also split halos based on percentiles of local overdensity.

The reason we explore both is to test whether the galaxy distribution is affected specifically by the tidal environment or whether the conclusions drawn in that case hold true in the case of splitting galaxies into different density regions as well.

4.3.1 Tidal environment

To characterize the “cosmic web” distribution in our simulation, we follow the conventional tidal environment assignment algorithm (Doroshkevich 1970; Hahn et al. 2007; Forero-Romero et al. 2009). First, we evaluate the density field, $\delta(\mathbf{x})$ using cloud-in-cell (CIC) interpolation on a 256^3 cubic lattice of only the dark matter particles. We then solve the Poisson equation $\nabla^2\psi = \delta$ and obtain the second derivative $\psi_{ij} \equiv \partial^2\psi/\partial x_i\partial x_j$ in Fourier space, applying a Gaussian smoothing kernel. Finally, we compute the eigenvalues $\lambda_1 \leq \lambda_2 \leq \lambda_3$ and define the 4 standard types of environment:

- **peaks:** all eigenvalues below the threshold ($\lambda_{\text{th}} \geq \lambda_1$)
- **filaments:** one eigenvalue below the threshold ($\lambda_1 \geq \lambda_{\text{th}} \geq \lambda_2$)
- **sheets:** two eigenvalues below the threshold ($\lambda_2 \geq \lambda_{\text{th}} \geq \lambda_3$)
- **voids:** all eigenvalues above the threshold ($\lambda_3 \geq \lambda_{\text{th}}$).

The choice of the threshold value for the eigenvalues is somewhat arbitrary. Here, we pick $\lambda_{\text{th}} = 1.2$ in order to maintain a roughly equal number of galaxies in the first three tidal environment types. A given halo is said to belong in one of four environment types depending on the environment type of the cell it is located in.

We apply the random shuffling procedure in Section 2.2 to each of the first three regions defined above (as the last region, the voids, turns out to have 0 galaxies for our choice of λ_{th} and galaxy definition). In Fig. 8, we show the results of this random shuffling in each region in 5% mass bins. We see that the galaxy clustering ratio on large scales when we fix the environment type and shuffle only within it is more consistent with full-physics TNG300-1 (differing from it by 4.8%, 1.1% and 4.0% in each of the three panels, respectively, for $r > 1$ Mpc/h). In our fiducial shuffling plot of all halos irrespective of their environments, i.e. Fig. 3, we saw a 15% difference, which implies that galaxies belonging to halos in one environment are likely resorted into halos residing in another tidal region. This suggests that for future models of galaxy occupation a split into environment regions might lead to better agreement between the mock galaxy catalogs and the true galaxy distribution.

4.3.2 Density percentiles

We now attempt yet another environment-based reshuffling scheme, this time parameterizing environment by $\mathbf{d}(\mathbf{x}) \equiv \log_{10}(1 + \delta(\mathbf{x}))$, where δ is the local overdensity computed in 4.3.1. We adopt the following ranges for the densest, second densest and third densest regions, respectively: $\mathbf{d} \in [0, 0.99)$, $\mathbf{d} \in [0.99, 1.3)$, and $\mathbf{d} \in [1.3, 3)$, *. We have investigated the

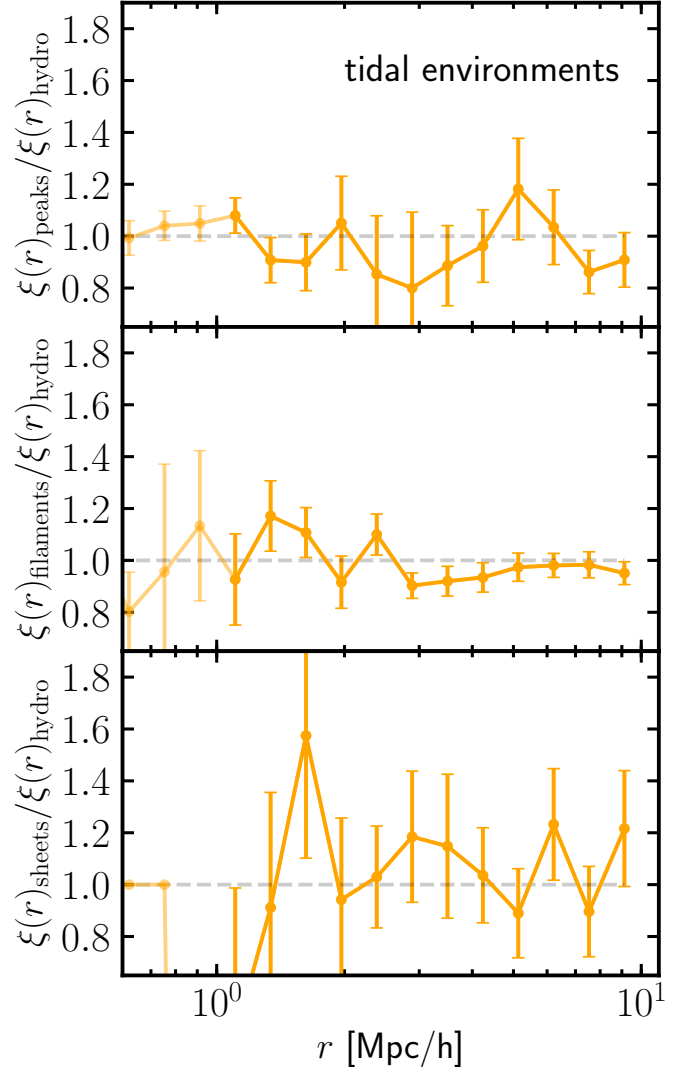


Figure 8. Correlation function ratio between the shuffled halo occupations in 5% mass bins and the fiducial (unshuffled) case for halos residing in the peaks *upper panel*, filaments *middle panel*, and sheets *lower panel*. This result exhibits a more modest discrepancy from the *hydro*simulation (*) result compared with what was observed in the full sample (Fig. 3) for $r > 1$ Mpc/h, where the difference between the hydrosimulation result and the “basic” HOD one is about 15%. There is roughly an equal number of galaxies residing in each of the three environments. This suggests that galaxies in halos of the same environment cluster similarly. The error bars are relatively large both because of the few objects and the limited volume occupied by the sheets and knots, in particular.

effect of random shuffling in 5% mass bins within each region. The 3D map of the DM density of TNG300 is obtained with a CIC assignment and pixel size of 205/256 Mpc/h \approx 0.8 Mpc/h. (Forero-Romero 2019).

Similarly to the previous case of classifying and shuffling within each tidal environment region, we will do the same for each density region, but first we need to pick bounds which define the density regions. As in the previous case, we will choose the boundary points arbitrarily, defined so as to preserve a roughly constant number of galaxies within

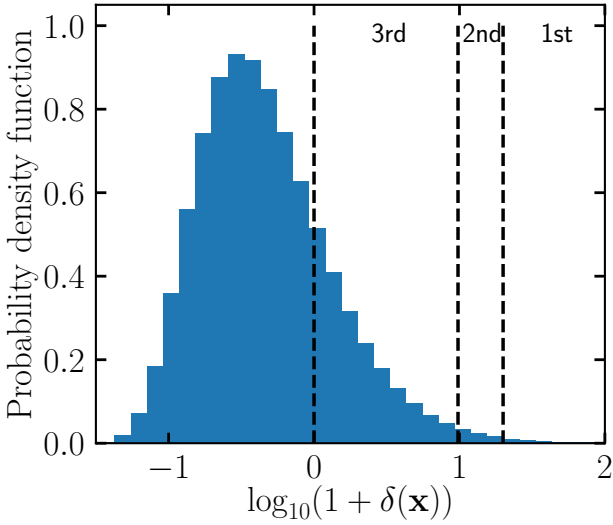


Figure 9. Histogram of the flattened 3D-logarithmic DM density in TNG300. The splits between the 3 regions are chosen such that each one contains a roughly equal number of galaxies as would be ascribed from the bijective matches with the hydrodynamical simulation.

each region (except the lowest density one). We then apply the methodology from Section 2.2. The results are shown in Fig. 10. The ratio is again nearly 1 which is far from the 15% discrepancy for $r > 1$ Mpc/h observed in the initial test we perform on TNG300 (differing from it by 3.0%, 3.2% and 1.8% in each of the three panels, respectively). We see a smaller scatter compared with the cosmic web definition 8, which is most likely because the volume which each of the density regions occupies is slightly less strictly defined than in the tidal environment case.

5 CONCLUSIONS

The standard galaxy-halo modeling based on the HOD methodology predicts that the number of galaxies residing in a halo is determined solely by its mass. Recent findings have challenged the assumptions of this model (Zehavi et al. 2019), hinting at discrepancies on large scales, e.g. when comparing the HOD-inferred result with weak lensing data (Leauthaud et al. 2017). In this paper, we put the standard HOD method to a test by generating a standard HOD galaxy sample and comparing it to the “true” galaxy distribution within the same hydrodynamical simulation, TNG300-1. By computing the correlation function of galaxies in the HOD catalog with those in the “true” case, we have shown (Fig. 3) that the simplest HOD model potentially leads to differences of order 15% at large scales (> 1 Mpc/h).

Before considering physical explanations for the observed large-scale discrepancy, we further tested the statistical rigor of our results. First, we have repeated the exercise on 27 N-body ABACUS boxes ($L_{\text{subbox}} = 240$ Mpc/h) (Garri-son et al. 2018c), but this time with purely HOD-assigned galaxies (see Fig. 5). The fact that Fig. 5 does not exhibit the same level of discrepancy as Fig. 3 implies that the observed 15% difference in the TNG simulation box is highly

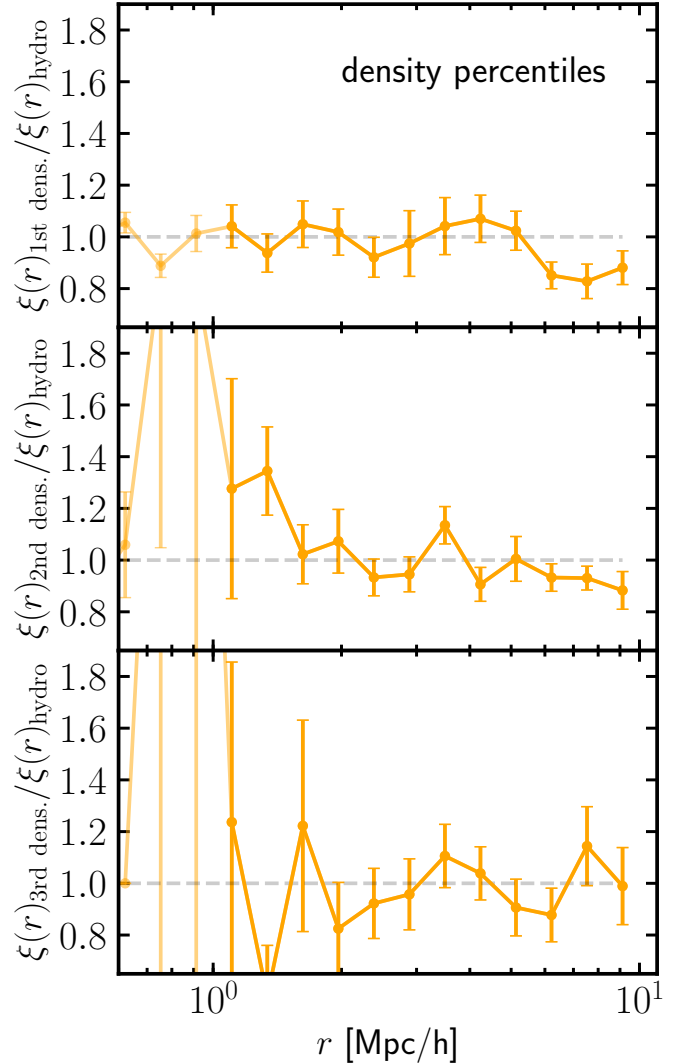


Figure 10. Correlation function ratio between the shuffled halo occupations in 5% mass bins and the fiducial (unshuffled) case for halos residing in the densest (*upper panel*), second densest (*middle panel*), and third densest (*lower panel*) regions. There is roughly an equal number of galaxies residing in each of the three environments. This result (a difference of 3.0%, 3.2% and 1.8%, respectively) does not exhibit a discrepancy at the level observed in the full sample (Fig. 3) (15% for $r > 1$ Mpc/h, which indicates that effects such as the environment density are vital for determining the galaxy occupation numbers of halos since halos in similar environments cluster similarly).

unlikely to be solely an artifact of the limited simulation volume. Another possible source of error may be in the choice of halo finder. TNG uses the group-finding technique FoF (Davis et al. 1985), which is typically preferred for on-the-fly implementations over alternative algorithms especially in high-resolution simulations, where computation time plays an important role. However, FoF is thought to be less accurate at finding halos (Lukić et al. 2009; More et al. 2011; Knebe et al. 2011), so we have instead run the alternative group-finder ROCKSTAR (Behroozi et al. 2013b), which, although slower, uses full phase-space information. This did not alleviate the issue at hand. We have also experimented

(see Table 1) with constructing the HOD using different halo mass proxies (such as M_{200m} , M_{200c} , and V_{peak}), and find that M_{200m} serves to minimise the large-scale differences. However, this is only at the 15% level, and does not diminish the differences in Fig. 3 entirely.

This 15% deviation could be reflective of an inherent issue with these models. The relationship between the galaxy and its parent halo mass is strong, but galaxies are also known to be biased tracers of the halo and total mass distributions, an effect known as “galaxy assembly bias”. While properties such as halo formation time, environment, concentration, triaxiality, spin, and velocity dispersion play a non-negligible role in the halo clustering, the relationship between the halo properties and that of the galaxy is not well understood. In this paper, we test 8 halo properties beyond mass — local environment, velocity anisotropy, $\sigma^2 R_{\text{halfmass}}$, velocity dispersion, halo spin, halo concentration, depth of the potential, and formation epoch — in an attempt to reveal which ones, if any, have a direct impact on the large-scale clustering of galaxies (see Table 2).

We find that halo environment correlates very strongly with the number of observed galaxies in it, which suggests that in order to obtain a galaxy distribution that better reproduces the clustering on large scales, it may be necessary take into consideration the environment in which the halo is embedded. We have further studied two different proxies for the environment factor – tidal environment and smoothed density field, shuffling the halos within their assigned regions. The result (shown in Fig. 8 and Fig. 10) is much less discrepant in that case compared with the full sample, which is another compelling piece of evidence suggesting that the inclusion of an environment parameter may be crucial to obtaining the correct clustering amplitude on large scales. The correlation between the ages of the galaxies and the ages of their dark matter halos has not yet been extensively studied in IllustrisTNG and thus remains an open question. If shown to be strong, it would also have an effect on the observed clustering in color-selected samples, for which there has already been evidence in the literature. We leave the study of color-dependent clustering in TNG (Nelson et al. 2018b) for a subsequent paper, realizing its potential as a systematic error that would need to be accounted for in redshift space distortions constraints coming from future surveys such as DESI (Levi et al. 2013).

Another important factor that may be at play is the effect of baryon physics processes on the matter distribution, which may contribute significantly to the bias between the halo and the galaxy distributions. To illustrate, it is possible that violent processes such as AGN feedback may expel enough material to cause the intrinsic properties of a halo, such as its concentration, to vary considerably between the dark-matter only and the hydrodynamical simulations. If this hypothesis is true, then extracting the properties of halos from N-body simulations in order to generate mock galaxy catalogs might lead to certain issues and the effect of baryonic physics would need to somehow be accounted for in the final N-body products.

Since the large-scale clustering obtained from the IllustrisTNG 300 Mpc simulation box matches the clustering of real galaxies reasonably well (Springel et al. 2018), we can conclude from our results that the basic HOD model for assigning galaxies to halos in an N-body simulation in-

troduces too significant of a discrepancy on large scales to meet the required level of accuracy for upcoming experiments. We, therefore, suggest a possible direction for alleviating this problem – namely, by including secondary halo parameters (assembly bias parameters), in addition to mass, to the HOD model. However, the design of a viable model that would improve the precision to the required $\sim 1\%$ level is left for future work.

The availability of an even larger hydrodynamical galaxy formation simulation would be extremely beneficial to expanding our knowledge of the relationship between galaxies and their dark matter halos. It would not only allow us to check and verify the results obtained with TNG300-1, but also provide us with substantially more objects. We would have a sufficiently large dataset to draw conclusions about the large-scale structure of the Universe with a high degree of confidence, possibly including tertiary parameters to the HOD model to capture the behavior even better. Finally, we hope that it would open the doors for creating improved HOD models that recover the galaxy clustering on large scales with subpercentage precision – a feat that could bridge important gaps in light of future galaxy surveys.

ACKNOWLEDGEMENTS

We thank Volker Springel, Benedikt Diemer, Kai Hoffman and the referee Darren Croton for their illuminating and useful comments. The IllustrisTNG data used in this paper is stored on the FASRC Cannon cluster supported by the FAS Division of Science Research Computing Group at Harvard University. DJE is supported by U.S. Department of Energy grant DE-SC0013718 and as a Simons Foundation Investigator. The Flatiron Institute is supported by the Simons Foundation.

REFERENCES

- Abbas U., Sheth R. K., 2007, *Mon. Not. R. Astron. Soc.*, **378**, 641
 Adhikari S., Dalal N., Chamberlain R. T., 2014, *Journal of Cosmology and Astroparticle Physics*, **11**, 019
 Artale M. C., Zehavi I., Contreras S., Norberg P., 2018, *Mon. Not. R. Astron. Soc.*, **480**, 3978
 Behroozi P. S., Wechsler R. H., Wu H.-Y., 2013a, *ApJ*, **762**, 109
 Behroozi P. S., Wechsler R. H., Wu H.-Y., 2013b, *ApJ*, **762**, 109
 Beltz-Mohrmann G. D., Berlind A. A., Szewciw A. O., 2019, arXiv e-prints, p. [arXiv:1908.11448](https://arxiv.org/abs/1908.11448)
 Benson A. J., 2017, *Mon. Not. R. Astron. Soc.*, **471**, 2871
 Berlind A. A., Weinberg D. H., 2002, *Astrophys. J.*, **575**, 587
 Bett P., Eke V., Frenk C. S., Jenkins A., Helly J., Navarro J., 2007, *Mon. Not. R. Astron. Soc.*, **376**, 215
 Binney J., Tremaine S., 1987, *Galactic dynamics*
 Blumenthal G. R., Faber S. M., Primack J. R., Rees M. J., 1984, *Nature*, **311**, 517
 Bose S., Eisenstein D. J., Hernquist L., Pillepich A., Nelson D., Marinacci F., Springel V., Vogelsberger M., 2019, arXiv e-prints, p. [arXiv:1905.08799](https://arxiv.org/abs/1905.08799)
 Bullock J. S., Kolatt T. S., Sigad Y., Somerville R. S., Kravtsov A. V., Klypin A. A., Primack J. R., Dekel A., 2001a, *Mon. Not. R. Astron. Soc.*, **321**, 559
 Bullock J. S., Dekel A., Kolatt T. S., Kravtsov A. V., Klypin A. A., Porciani C., Primack J. R., 2001b, *ApJ*, **555**, 240
 Cooray A., 2002, *ApJ*, **576**, L105

- Croton D. J., Gao L., White S. D. M., 2007, *Mon. Not. R. Astron. Soc.*, **374**, 1303
- Dalal N., Doré O., Huterer D., Shirokov A., 2008, *Phys. Rev. D*, **77**, 123514
- Davis M., Efstathiou G., Frenk C. S., White S. D. M., 1985, *ApJ*, **292**, 371
- Diemer B., 2017, *The Astrophysical Journal Supplement Series*, **231**, 5
- Diemer B., Kravtsov A. V., 2014, *ApJ*, **789**, 1
- Diemer B., Kravtsov A. V., 2015, *ApJ*, **799**, 108
- Diemer B., Mansfield P., Kravtsov A. V., More S., 2017, *ApJ*, **843**, 140
- Dolag K., Komatsu E., Sunyaev R., 2016, *Mon. Not. R. Astron. Soc.*, **463**, 1797
- Doroshkevich A. G., 1970, *Astrophysics*, **6**, 320
- Dubois Y., et al., 2014, *Mon. Not. R. Astron. Soc.*, **444**, 1453
- Fakhouri O., Ma C.-P., 2009, *Mon. Not. R. Astron. Soc.*, **394**, 1825
- Fakhouri O., Ma C.-P., 2010, *Mon. Not. R. Astron. Soc.*, **401**, 2245
- Faltenbacher A., White S. D. M., 2010, *ApJ*, **708**, 469
- Forero-Romero J. E., 2019, IllustrisWeb, <https://github.com/forero/IllustrisWeb>
- Forero-Romero J. E., Hoffman Y., Gottlöber S., Klypin A., Yepes G., 2009, *Mon. Not. R. Astron. Soc.*, **396**, 1815
- Gao L., White S. D. M., 2007, *Mon. Not. R. Astron. Soc.*, **377**, L5
- Gao L., Springel V., White S. D. M., 2005, *Mon. Not. R. Astron. Soc.*, **363**, L66
- Garcia R., Rozo E., 2019, arXiv e-prints, p. [arXiv:1903.01709](https://arxiv.org/abs/1903.01709)
- Garrison L. H., Eisenstein D. J., Ferrer D., Metchnik M. V., Pinto P. A., 2016, *Mon. Not. R. Astron. Soc.*, **461**, 4125
- Garrison L. H., Eisenstein D. J., Ferrer D., Tinker J. L., Pinto P. A., Weinberg D. H., 2018a, *The Astrophysical Journal Supplement Series*, **236**, 43
- Garrison L. H., Eisenstein D. J., Ferrer D., Tinker J. L., Pinto P. A., Weinberg D. H., 2018b, *The Astrophysical Journal Supplement Series*, **236**, 43
- Garrison L. H., Eisenstein D. J., Ferrer D., Tinker J. L., Pinto P. A., Weinberg D. H., 2018c, *The Astrophysical Journal Supplement Series*, **236**, 43
- Genel S., et al., 2014, *Mon. Not. R. Astron. Soc.*, **445**, 175
- Hahn O., Porciani C., Carollo C. M., Dekel A., 2007, *Mon. Not. R. Astron. Soc.*, **375**, 489
- Johnson J. W., Maller A. H., Berlind A. A., Sinha M., Holley-Bockelmann J. K., 2019, *Mon. Not. R. Astron. Soc.*, **486**, 1156
- Knebe A., et al., 2011, *Mon. Not. R. Astron. Soc.*, **415**, 2293
- Lacerna I., Padilla N., 2012, *Mon. Not. R. Astron. Soc.*, **426**, L26
- Lacerna I., Padilla N., Stasyszyn F., 2014, *Mon. Not. R. Astron. Soc.*, **443**, 3107
- Landy S. D., Szalay A. S., 1993, *ApJ*, **412**, 64
- Leauthaud A., et al., 2017, *Mon. Not. R. Astron. Soc.*, **467**, 3024
- Levi M., et al., 2013, arXiv e-prints, p. [arXiv:1308.0847](https://arxiv.org/abs/1308.0847)
- Lewis A., Challinor A., 2011, CAMB: Code for Anisotropies in the Microwave Background, Astrophysics Source Code Library (ascl:1102.026)
- Lovell M. R., et al., 2018, *Mon. Not. R. Astron. Soc.*, **481**, 1950
- Ludlow A. D., Navarro J. F., Angulo R. E., Boylan-Kolchin M., Springel V., Frenk C., White S. D. M., 2014, *Mon. Not. R. Astron. Soc.*, **441**, 378
- Ludlow A. D., Bose S., Angulo R. E., Wang L., Hellwing W. A., Navarro J. F., Cole S., Frenk C. S., 2016, *Mon. Not. R. Astron. Soc.*, **460**, 1214
- Lukić Z., Reed D., Habib S., Heitmann K., 2009, *ApJ*, **692**, 217
- Mansfield P., Kravtsov A. V., 2019, arXiv e-prints, p. [arXiv:1902.00030](https://arxiv.org/abs/1902.00030)
- Marinacci F., et al., 2018, *Mon. Not. R. Astron. Soc.*, **480**, 5113
- McCarthy I. G., Schaye J., Bird S., Le Brun A. M. C., 2017, *Mon. Not. R. Astron. Soc.*, **465**, 2936
- Merritt D., 1987, *ApJ*, **313**, 121
- More S., Kravtsov A. V., Dalal N., Gottlöber S., 2011, *ApJS*, **195**, 4
- More S., Diemer B., Kravtsov A. V., 2015, *ApJ*, **810**, 36
- Naiman J. P., et al., 2018, *Mon. Not. R. Astron. Soc.*, **477**, 1206
- Navarro J. F., Frenk C. S., White S. D. M., 1996, *ApJ*, **462**, 563
- Navarro J. F., Frenk C. S., White S. D. M., 1997, *ApJ*, **490**, 493
- Nelson D., et al., 2018b, *Mon. Not. Roy. Astron. Soc.*, **475**, 624
- Nelson D., et al., 2018a, *Mon. Not. R. Astron. Soc.*, **475**, 624
- Nelson D., et al., 2019a, *Mon. Not. R. Astron. Soc.*
- Nelson D., et al., 2019b, *Computational Astrophysics and Cosmology*, **6**, 2
- Norberg P., et al., 2001, *Mon. Not. R. Astron. Soc.*, **328**, 64
- Oñorbe J., Garrison-Kimmel S., Maller A. H., Bullock J. S., Rocha M., Hahn O., 2014, *Mon. Not. R. Astron. Soc.*, **437**, 1894
- Paranjape A., Hahn O., Sheth R. K., 2018, *Mon. Not. R. Astron. Soc.*, **476**, 5442
- Peacock J. A., Smith R. E., 2000, *Mon. Not. R. Astron. Soc.*, **318**, 1144
- Pillepich A., et al., 2018a, *Mon. Not. R. Astron. Soc.*, **473**, 4077
- Pillepich A., et al., 2018b, *Mon. Not. R. Astron. Soc.*, **475**, 648
- Pillepich A., et al., 2019, *Mon. Not. R. Astron. Soc.*
- Pujol A., Gaztañaga E., 2014, *Mon. Not. R. Astron. Soc.*, **442**, 1930
- Pujol A., Hoffmann K., Jiménez N., Gaztañaga E., 2017, *A&A*, **598**, A103
- Ramakrishnan S., Paranjape A., Hahn O., Sheth R. K., 2019, arXiv e-prints, p. [arXiv:1903.02007](https://arxiv.org/abs/1903.02007)
- Rodríguez-Puebla A., Behroozi P., Primack J., Klypin A., Lee C., Hellinger D., 2016, *Mon. Not. R. Astron. Soc.*, **462**, 893
- Schaller M., et al., 2015, *Mon. Not. R. Astron. Soc.*, **451**, 1247
- Scoccimarro R., Sheth R. K., Hui L., Jain B., 2001, *ApJ*, **546**, 20
- Seljak U., 2000, *Mon. Not. R. Astron. Soc.*, **318**, 203
- Shi J., Sheth R. K., 2018, *Mon. Not. R. Astron. Soc.*, **473**, 2486
- Springel V., 2010, *Mon. Not. R. Astron. Soc.*, **401**, 791
- Springel V., White S. D. M., Tormen G., Kauffmann G., 2001, *Mon. Not. Roy. Astron. Soc.*, **328**, 726
- Springel V., et al., 2018, *Mon. Not. R. Astron. Soc.*, **475**, 676
- Vogelsberger M., et al., 2014a, *Mon. Not. R. Astron. Soc.*, **444**, 1518
- Vogelsberger M., et al., 2014b, *Nature*, **509**, 177
- Wang H., Mo H. J., Jing Y. P., 2009, *Mon. Not. R. Astron. Soc.*, **396**, 2249
- Wechsler R. H., Bullock J. S., Primack J. R., Kravtsov A. V., Dekel A., 2002, *Astrophys. J.*, **568**, 52
- Wechsler R. H., Zentner A. R., Bullock J. S., Kravtsov A. V., Allgood B., 2006, *ApJ*, **652**, 71
- Weinberger R., et al., 2017, *Mon. Not. R. Astron. Soc.*, **465**, 3291
- Weinberger R., Springel V., Pakmor R., 2019, arXiv e-prints, p. [arXiv:1909.04667](https://arxiv.org/abs/1909.04667)
- White S. D. M., Rees M. J., 1978, *Mon. Not. R. Astron. Soc.*, **183**, 341
- Yang X., Mo H. J., Jing Y. P., van den Bosch F. C., Chu Y., 2004, *Mon. Not. R. Astron. Soc.*, **350**, 1153
- Zehavi I., et al., 2002, *ApJ*, **571**, 172
- Zehavi I., Contreras S., Padilla N., Smith N. J., Baugh C. M., Norberg P., 2018, *ApJ*, **853**, 84
- Zehavi I., Kerby S. E., Contreras S., Jiménez E., Padilla N., Baugh C. M., 2019, arXiv e-prints, p. [arXiv:1907.05424](https://arxiv.org/abs/1907.05424)
- Zheng Z., et al., 2005, *Astrophys. J.*, **633**, 791

This paper has been typeset from a $\text{\TeX}/\text{\LaTeX}$ file prepared by the author.